106 *Chem. Mater.* **2011,** *23,* 106–113
DOI:10.1021/cm102136f

CHEMISTRY OF MATERIALS
Article

Sol−Gel Synthesis of High-Quality $SrRuO_3$ Thin-Film Electrodes Suppressing the Formation of Detrimental RuO_2 and the Dielectric Properties of Integrated Lead Lanthanum Zirconate Titanate Films

Manoj Narayanan,*,† Sheng Tong,† Rachel Koritala,‡ Beihai Ma,† Vilas G. Pol,§ and U. Balachandran†

†*Energy Systems Division,* ‡*Materials Science Division, and* §*Chemical Sciences & Engineering Division, Argonne National Laboratory, Argonne, Illinois 60439, United States*

Received July 30, 2010. Revised Manuscript Received October 5, 2010

A facile solution chemistry is demonstrated to fabricate high-quality polycrystalline strontium ruthenium oxide ($SrRuO_3$) thin film electrodes on silicon substrates suppressing the formation of undesired ruthenium oxide (RuO_2) for the deposition of dielectric and ferroelectric materials like lead lanthanum zirconate titanate (PLZT). The robust, highly crystalline $SrRuO_3$ film fabrication process does not favor the formation of RuO_2 because of molecular level modification of the precursors possessing analogous melting points, yielding homogeneous films. This chemistry is further understood and complemented by kinetic and thermodynamic analysis of the DTA data under non-isothermal conditions, with which the activation energies to form RuO_2 and $SrRuO_3$ were calculated to be 156 ± 17 and 96 ± 10 kJ/mol, respectively. The room-temperature resistivity of the $SrRuO_3$ film was measured to be $\sim 850 \pm 50$ $\mu\Omega$ cm on silicon (100) substrates. The dielectric properties of sol−gel-derived PLZT thin film capacitors on polycrystalline $SrRuO_3$ electrodes were also measured to illustrate the high quality of the formed $SrRuO_3$ bottom electrode. These results have broad implications for the expanded use of these conductive oxide electrodes in many applications that require low thermal budgets. The PLZT (8/52/48) films exhibited well-defined hysteresis loops with remanent polarization of ~ 10.5 $\mu C/cm^2$, dielectric constant of > 1450, dielectric loss of < 0.06, and leakage current density of $\sim 3.8 \times 10^{-8}$ A/cm^2. These dielectric properties are similar to those of PLZT on platinized silicon, indicating the high quality of the bottom conductive oxide layer. In addition, the PLZT capacitors were essentially fatigue free for $> 1 \times 10^9$ cycles when deposited over an oxide electrode.

1. Introduction

During the last two decades, the strontium ruthenium oxide ($SrRuO_3$ or SRO) thin film electrodes received considerable attention because of their high metallic conductivity[1,2] and high temperature stability (1200 K or 927 °C) in oxidizing or inert atmospheres,[3] making them suitable in numerous technological applications. Moreover, SRO films improve the fatigue and imprint behavior of ferroelectric materials such as barium strontium titanate (BST)[4] and lead lanthanum zirconate titanate (PLZT), because of their small lattice mismatch. Therefore, SRO films are ideal as a conductive electrode and/or buffer layer to grow epitaxial ferroelectric thin films in many applications including dynamic RAM and ferroelectric RAM. The reported room-temperature resistivity of SRO thin film formed by physical vapor deposition techniques is on the order of 1×10^{-4} Ω cm that was employed as an electrode in several oxide-based devices.[1,2] At room temperature, SRO perovskite crystallizes in the orthorhombic structure with space group *Pbnm* and lattice parameters $a = 5.5730$ Å, $b = 5.5381$ Å, and $c = 7.856$ Å. This structure is a slightly distorted pseudocubic perovskite with unit cell parameter[5] $a_c = 3.93$ Å, presenting excellent structural compatibility with many perovskite-based ferroelectric oxides.

Considering various applications of SRO films, extensive efforts have been devoted to depositing device-quality SRO thin films on (100)Si, (100)$SrTiO_3$, (100)$LaAlO_3$, and (100)MgO substrates through expensive and complicated techniques like RF sputtering,[1,6] pulsed laser deposition (PLD),[2,7,8] dc magnetron sputtering,[9] and metal−organic

*Corresponding author. Tel: +1-(630) 252-6856. Fax: +1-(630) 252-3604. E-mail: mnarayanan@anl.gov.

(1) Eom, C. B.; Cava, R. J.; Fleming, R. M.; Philips, J. M.; Van Dover, R. B.; Marshall, J. H.; Hsu, J. W.; Krajewski, J. J.; Peck, W. F. *Science* **1992**, *258*, 1766.
(2) Herranz, G.; Sánchez, F.; Fontcuberta, J.; García-Cuenca, M. V.; Ferrater, C.; Varela, M.; Angelova, T.; Cros, A.; Cantarero, A. *Phys. Rev. B* **2005**, *71*, 174411.
(3) Eom, C. B.; Van Dover, R. B.; Philips, J. M.; Werder, D. J.; Marshall, J. H.; Chen, C. H.; Cava, R. J.; Fleming, R. M. *Appl. Phys. Lett.* **1993**, *63*, 2570.
(4) Izuha, M.; Abe, K.; Koike, M.; Takeno, S.; Fukushima, N. *Appl. Phys. Lett.* **1997**, *70*, 1405.
(5) Mercurio, J. P.; Yi, J. H.; Manier, M.; Thomas, P. *J. Alloys Compd.* **2000**, *308*, 77.
(6) Rao, R. A.; Gan, Q.; Eom, C. B. *Appl. Phys. Lett.* **1997**, *71*, 1171.
(7) Qin, W. F.; Ai, W. Y.; Zhu, J.; Xiong, J.; Tang, J.; Zhang, Y.; Li, Y. R. *J. Mater. Sci.* **2007**, *42*, 8707.
(8) Zakharov, N. D.; Satyalakshmi, K. M.; Koren, G.; Hesse, D. *J. Mater. Res.* **1999**, *14*, 4385.

 Published on Web 12/15/2010 © 2010 American Chemical Society

chemical vapor deposition (MOCVD).[10,11] Mercurio et al.[5] used metal−organic decomposition to form SRO powders and films on silicon substrates with different precursors, which consisted of an unidentified impurity (secondary phases) and RuO_2. Moreover, the fabricated SRO films on silicon substrates were randomly oriented. Seveno et al.[12] deposited SRO films on steel substrates and concluded that the process is sensitive to the pyrolysis and crystallization temperatures. They also reported on the decomposition of ruthenium nitrosyl nitrate precursor to RuO_2 at temperatures as low as 260 °C. At such low pyrolysis temperatures, incomplete organic removal inhibited the formation of the metal−oxygen−metal (M−O−M) gel network. Additionally, the obtained RuO_2 phase did not change during the final crystallization anneal even at higher temperatures. Suzuki et al.[13] employed strontium metal and strontium chloride precursors to fabricate SRO films with resistivity of 1100−20000 $\mu\Omega$ cm. However, chlorine-containing precursor compounds are typically detrimental to the electrical properties and are not favored in solution processing.

Though few articles have reported on the fabrication of SRO thin films using chemical solution deposition (CSD),[5,12,13] none of them reported on the electrical quality of the obtained films. Very little attention was paid to economically viable sol−gel-based CSD. Additionally, the presence of undesired ruthenium oxide (RuO_2) phases was mostly observed in previous efforts.[5,12,13] Therefore, a facile process to achieve pure phase of SRO thin films by sol−gel synthesis with good electrical properties is extremely important.

In this effort, we successfully developed novel solution chemistry with robust crystallization conditions to fabricate SRO thin films without the formation of undesired RuO_2 or secondary phases by appropriate choice of precursors. We studied the structural evolution of the films using differential thermal analysis and X-ray diffraction. Electrical characterization of the fabricated SRO films was conducted on silicon substrates, and their integrity as a bottom electrode was tested by characterizing the dielectric properties of PLZT films deposited over the SRO bottom electrode. In microelectronics, the device performance is strongly related to the microstructure and the electrical resistivity of the SRO thin films; therefore, this study is crucial for the fabrication of a functional bottom electrode.

2. Experimental Section

A 0.2 M SRO solution was made by first dissolving stochiometric ruthenium(III) nitrosyl nitrate $[Ru(NO)(NO_3)_3]$ (Alfa Aesar, Ward Hill, MA) in 2-methoxyethanol $[CH_3OCH_2CH_2OH]$ (2-MOE) (>99.9%, Sigma-Aldrich, St.Louis, MO) and strontium acetate hydrate $[Sr(OCOCH_3)_2.xH_2O]$ (99.995%, Aldrich, St. Louis, MO) in glacial acetic acid $[CH_3COOH]$ (Fisher Scientific, Fair Lawn, NJ) at room temperature. These two individual solutions were then mixed together for 2 h at room temperature, forming a uniform brown solution. This SRO stock solution was used to spin coat onto Si (100) substrates through a 0.02 μm Whatman in-line filter. The SRO solution was spin coated onto the substrate at 3000 rpm for 30 s, pyrolyzed at 450 °C for 10 min, and crystallized at 600−750 °C for 5 min. This sequence was repeated five times followed by a final annealing for 20 min at that temperature. The solution is clear and stable without any precipitation for 4−5 days and there was no noticeable solution aging effect on the observed microstructure and electrical properties.

Differential thermal analysis (DTA) was carried out on constituent precursor solutions and SRO solution by heating them up to 800 °C in air with a heating rate of 10 °C/min to develop the mechanistic understanding behind the homogeneous solution formation. The phase development of the films was studied with a Bruker AXS D8 diffraction system. Microstructure and thickness were characterized with a Hitachi S-4700-II field-emission scanning electron microscope (SEM). Platinum top electrodes (250-μm diameter and 100-nm thickness) were then deposited by electron beam evaporation through a shadow mask. Resistivity was measured by the four-point probe method using a Keithley 237 current source meter and Keithley 6517 electrometer. Optimized crystallization conditions, which resulted in the lowest-resistivity SRO films on silicon substrates, were used in subsequent experiments.

Optimized SRO films were deposited on Si (100) substrates followed by the deposition of PLZT dielectric films. A stock solution of 0.5 M $Pb_{0.92}La_{0.08}Zr_{0.52}Ti_{0.48}O_3$ (PLZT 8/52/48) was prepared by modified sol−gel synthesis using 2-methoxyethanol as the solvent. Details on the solution synthesis and thin film deposition of PLZT are reported elsewhere.[14−16] After platinum top electrodes were deposited, dielectric measurements were made with an Agilent E4980A LCR meter using an oscillator level of 0.1 V at 10kHz in conjunction with a Signatone QuieTemp probe station (Lucas Signatone Corp., Gilroy, CA). A Keithley 237 high-voltage source meter and Radiant Technologies Precision Premier II tester were used to measure the leakage current and polarization field (P-E) hysteresis loops. Polarization fatigue measurements were carried out using a 130 kV/cm and 50 kHz square waveform for $> 1 \times 10^9$ cycles. Data were collected automatically by programming the Vision software in the Premier II tester. All dielectric measurements were made with a top-electrode to top-electrode (two similar capacitors in series) configuration.

3. Results and Discussion

The proper choice of precursors and solvents are highly important to develop a robust synthetic technique since they ultimately determine the extent of intermixing of metal species, gel-network or individual inorganic phase formation. It will also determine the reaction kinetics, processing temperature, crystallization behavior, densification, microstructure or required phase formation,

(9) Sim, J. S.; Zhao, J. S.; Lee, H. J.; Lee, K.; Hwang, G. W.; Hwang, C. S. *J. Electrochem. Soc.* **2006**, *153*, C777.
(10) Okuda, N.; Saito, K.; Funakubo, H. *Jpn. J. Appl. Phys.* **2000**, *39*, 572.
(11) Lee, H. C.; Tsai, D. S. *J. Mater. Sci.* **2003**, *38*, 2633.
(12) Seveno, R.; Braud, A.; Gundel, H. W. *Thin Solid Films* **2005**, *493*, 124.
(13) Suzuki, H.; Miwa, Y.; Miyazaki, H.; Takahashi, M.; Ota, T. *Ceram. Int.* **2004**, *30*, 1357.
(14) Ma, B.; Kwon, D. K.; Narayanan, M.; Balachandran, U. *J. Electroceram.* **2009**, *22*, 383.
(15) Ma, B.; Narayanan, M.; Balachandran, U. *Mater. Lett.* **2009**, *63*, 1353.
(16) Narayanan, M.; Ma, B.; Balachandran, U.; Li, W. *J. Appl. Phys.* **2010**, *107*, 024103.

which will result in the final properties of the films. The chemical stability of the precursor solution is a key element in avoiding phase segregation at various stages of the oxide film formation. However, the choice of a suitable starting precursor and solvent for the synthesis of SRO is not obvious. For example, most of the readily soluble ruthenium compounds contain chloride ions, which deteriorate the electrical properties of the deposited film. It is also evident that, once introduced into the solution, these chloride ions are not completely removed.

Considering the related drawbacks, ruthenium nitrosyl nitrate and strontium acetate were selected as the precursors because of their stability and their complete solubility in 2-methoxyethanol and acetic acid, respectively. It should be pointed out that the choice of these two solvents (methoxyethanol and acetic acid) were also based on the fact that they possess similar boiling points (~125 and ~117 °C, respectively), which would assist to keep the homogeneity of the admixtures and minimize the probability of an individual M−O−M formation during pyrolysis. The formed homogeneous solution at the molecular level decreases the occurrence of phase segregation during spinning, pyrolysis, or crystallization. This claim is further substantiated by the nature of acetic acid, which is a weaker chelating agent than the acetylacetonate. Therefore, the acetate ligand is easier to remove (organic extraction) during pyrolysis due to their smaller hydrocarbon chain, facilitating the obvious M−O−M gel network formation. As a result, strontium acetate remained an excellent precursor in the preparation of BST thin films with acetic acid.[17−19] In summary, in our present synthetic approach for precursors, metallic precursors with longer chain ligands and chloride-based precursors were avoided. From the solvent point of view, acetic acid was chosen because it does not require aggressive pyrolysis conditions while fabricating SRO films.

To support our present mechanistic elucidation, the differential thermal analysis (DTA) of an individual ruthenium-MOE, strontium-acetic acid, and a mixture of both solutions (SRO) are presented in Figure 1. All the DTA experiments were carried out in an air atmosphere to further correlate the annealing conditions used for the pyrolysis and crystallization of the thin films. In all three solutions, the measured very broad endothermic peak is centered at around ~160 °C, resulting from the loss of water molecules.

The exotherm at ~300 °C confirms the decomposition of ruthenium-MOE solution (Figure 1a), while the strontium-acetic acid solution decomposes at ~435 °C (Figure 1b).[20] These exothermic peaks are in good agreement with the literature attributing to the decomposition[20] and combustion

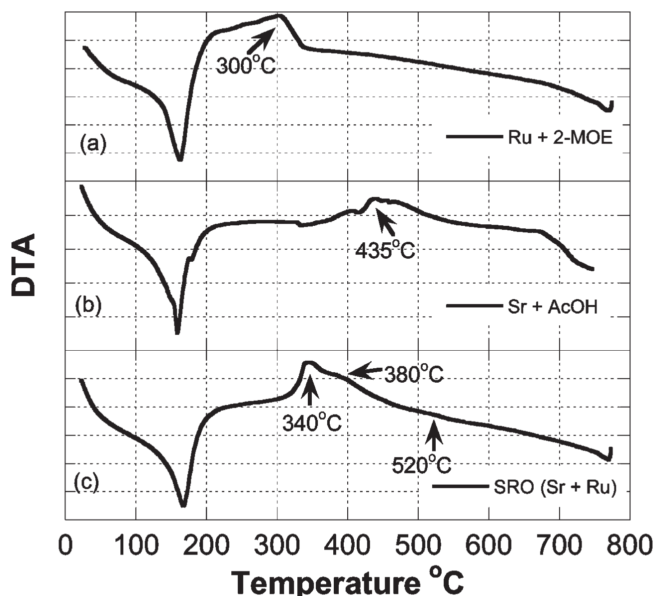

Figure 1. Differential thermal analysis of (a) ruthenium nitrosyl nitrate in 2-MOE, (b) strontium acetate in acetic acid, (c) SRO stock solution containing both a and b.

of organics (acetate ligands) for the respective compounds. As expected, the admixture of ruthenium-MOE and strontium-acetic acid solutions showed two exotherms at 340 and 380 °C (Figure 1c) in-between the exotherms of the two individual solutions. The peak positions of SRO solution (Figure 1c) indicated the modification of the individual precursor solutions at molecular level after mixing to form a homogeneous solution containing both the metallic species. In SRO solution, the difference between the two exothermic peaks is ~40 °C, which is lower than that between the individual decomposition events (~135 °C), indicating a different transformation pathway occurring for the SRO gel-network. Certainly, the thermodynamic stabilities of SRO solution are higher than the ruthenium-MOE solution forming a homogeneous network with strontium-acetic acid solutions, ultimately homogenizing uniformly the ruthenium and strontium cations. All these findings suggest a lower chance of individual phase segregation. In SRO solution, the small exothermic kink at around 520 °C (Figure 1c) is attributed to the conversion of amorphous to crystalline SRO. This observation further supported by the XRD measurements of the SRO films.

Previously, the RuO_2 phase has been reported to form at temperatures as low as 260 °C[20] and remain unaltered after exposure to crystallization temperatures of around 750 °C while processing SRO thin films.[12] This is a concern because the typical pyrolysis temperature used to obtain dense thin films by burning away organics in sol−gel synthesis ranges from 300 to 450 °C (depending on solution chemistry). In addition, incomplete organic removal inhibits the formation of M−O−M gel network. To further understand the nucleation and growth process in SRO, we deposited films on silicon substrates using ruthenium-MOE and SRO solution at 450 °C, where one would expect the formation of the more stable RuO_2 that has been reported in the literature.[5,20] X-ray diffraction

(17) Schwartz, R. W.; Clem, P. G.; Voigt, J. A.; Byhoff, E. R.; Stry, M. V.; Headley, T. J.; Missert, N. A. *J. Am. Ceram. Soc.* **1999**, *82*, 2359.
(18) Cheng, J. G.; Tang, J.; Chu, J. H.; Zhang, A. J. *Appl. Phys. Lett.* **2000**, *77*, 1035.
(19) Majumder, S. B.; Jain, M.; Martinez, A.; Katiyar, R. S.; Van Keuls, F. W.; Miranda, F. A. *J. Appl. Phys.* **2001**, *90*, 896.
(20) Yi, J. H.; Thomas, P.; Manier, M.; Mercurio, J. P. *J. Phys. IV France* **1998**, *8*, Pr9–45.

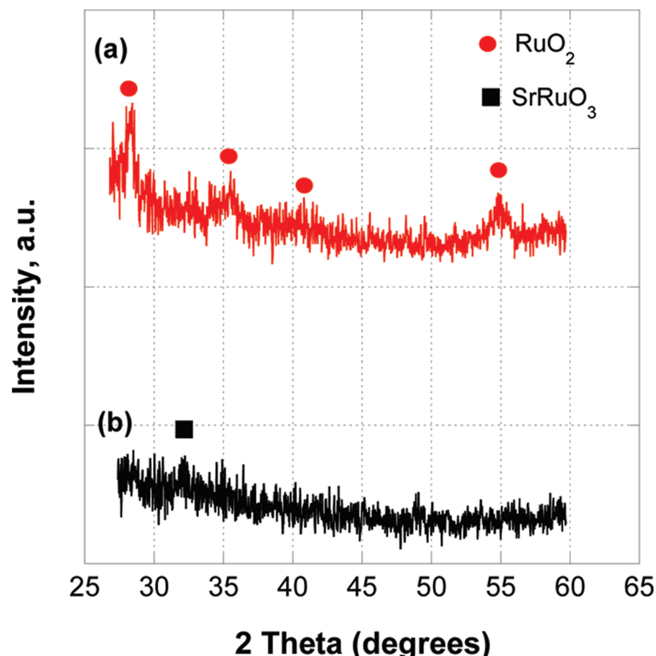

Figure 2. X-ray diffraction patterns of films formed by heat treatment at 450 °C using (a) ruthenium nitrosyl nitrate in 2-MOE and (b) SRO stock solution.

(XRD) of such films was performed to characterize the different phases or intermediate phases that developed and/or were converted to the required SRO phase.

The XRD patterns of various films formed by heat treatment at 450 °C using ruthenium nitrosyl nitrate in 2-MOE and SRO solutions are illustrated in panels a and b in Figure 2, respectively. As evident in Figure 2a (filled circles), the RuO_2 peaks can be clearly identified (JCPDS 21−1172) in the film made using ruthenium-MOE solution. This finding indicates the crystallization of RuO_2 even at such low temperatures, agreeing well with the published literature.[12,20] However, the RuO_2 diffraction peaks were not observed in the films made using SRO solution (Figure 2b) at the same temperature, which indicates that molecular modification of the precursor compounds to form a homogeneous solution, suppressing the RuO_2 formation. Figure 2b shows that the SRO films made at 450 °C were still amorphous in nature. From the Ellingham phase diagram for RuO_2−SRO,[21] we concluded that the oxygen partial pressure during processing has to be strictly controlled to obtain SRO without the presence of residual RuO_2 for temperatures < 800 °C. However, this was not observed in our case and substantiated by XRD results presented in Figure 4. To further understand why RuO_2 was not favored in SRO films made in air, we performed a kinetic analysis of the nonisothermal DTA data presented in parts a and c in Figure 1 and carried out thermodynamic calculations in the temperature range 200−450 °C, where the formation of crystalline RuO_2 and amorphous SRO was observed.

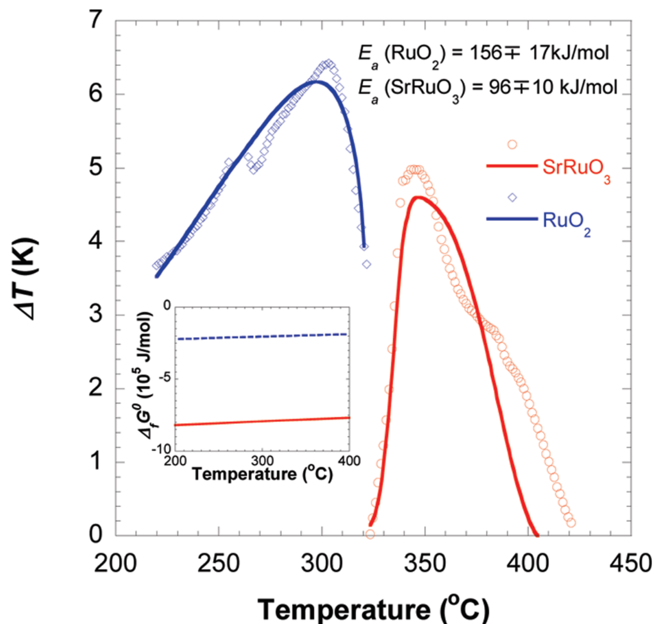

Figure 3. Measured and calculated ΔT for ruthenium nitrosyl nitrate in 2-MOE and SRO stock solution. Fits to data using eq 1 are shown as solid lines. The activation energies calculated from the fit to form RuO_2 and $SrRuO_3$ are 156 ± 17 and 96 ± 10 kJ/mol, respectively. Inset shows the Gibbs energy of formation for RuO_2 and $SrRuO_3$ calculated from refs 25−27 **in the same temperature range.**

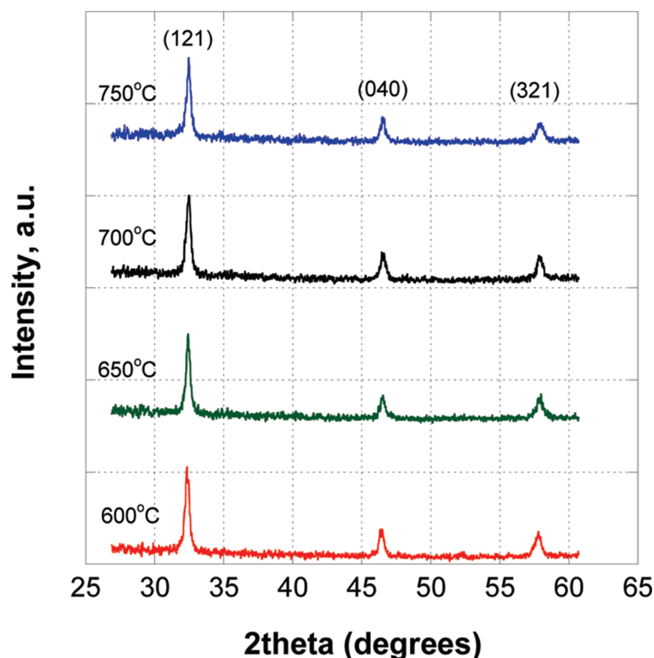

Figure 4. X-ray diffraction patterns of SRO films crystallized at different temperatures.

The DTA data were fit to curves with the reaction-order kinetic model reported by Malek et al.[22,23] to determine the activation energy required to form RuO_2 and SRO by using eq 1

$$\Delta T = A\exp\left(-\frac{E_a}{RT}\right)(1-\alpha)^n \tag{1}$$

(21) Shin, J.; Kalinin, S. V.; Lee, H. N.; Christen, H. M.; Moore, R. G.; Plummer, E. W.; Baddorf, A. P. *Surf. Sci.* **2005**, *581*, 118.

(22) Malek, J.; Criado, J. M. *Thermochim. Acta* **1992**, *203*, 25.
(23) Malek, J.; Criado, J. M. *Thermochim. Acta* **1994**, *236*, 187.

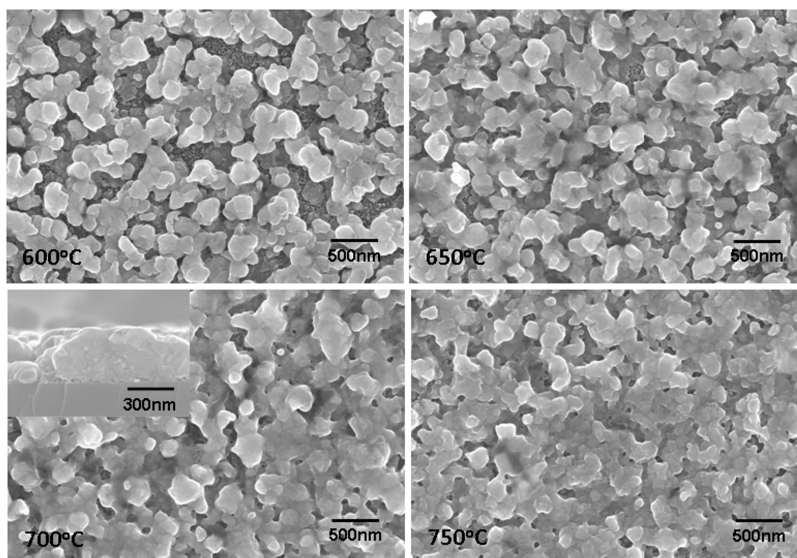

Figure 5. Scanning electron microscope images of SRO films crystallized at different temperatures. Inset shows the typical cross-section of the SRO film made at 700 °C.

In this equation, ΔT is the differential temperature between the reference and reactant solution in the DTA measurement (proportional to heat flow rate), A is a constant, E_a is the activation energy, R is the universal gas constant, α is the degree of conversion, and n is the order of the reaction. The degree of conversion is the ratio of area under the curve at certain temperature range to the whole area under the curve.[22-24] Figure 3 shows the DTA data along with the fit using eq 1. The r^2 values obtained for the fitted curves were greater than 0.99, indicating that the kinetic model matches very well with the measured data, as seen in the figure. The activation energies calculated from the fit for the formation of crystalline RuO_2 and amorphous SRO are 156 ± 17 and 96 ± 10 kJ/mol, respectively.

The inset in Figure 3 reveals the standard Gibbs energy of formation ($\Delta_f G^0$) for both RuO_2 and SRO, calculated from refs 25−27 for the temperature range 200−400 °C. Within this temperature range, $\Delta_f G^0$ (SRO) is always less than $\Delta_f G^0$ (RuO_2), and the activation energy to form SRO is smaller than RuO_2. These kinetic and thermodynamic analyses show that the reacted products in the solution favor the formation of SRO rather than RuO_2, indicating a robust process. Since ruthenium decomposition does not occur below 450 °C (Figure 2b), the pyrolysis temperature for the SRO thin films in further experiments was fixed at 450 °C to facilitate the complete removal of organics in the wet film. The crystallization temperature was set above 520 °C because of the crystallization peak observed at that temperature in Figure 1c.

The influence of annealing temperature on the crystallization behavior of the SRO films on silicon was studied by XRD. Figure 4 shows the diffraction patterns of films crystallized at temperatures ranging from 600 to 750 °C. Phase-pure polycrystalline SRO (JCPDS 43−0472) was formed at all temperatures without the presence of any residual RuO_2 phase. All the visible diffraction peaks can be indexed to SRO with relative intensities and positions in agreement with the JCPDS file. The lattice parameters calculated from the XRD peaks are a = 5.5319 Å, b = 5.4528 Å, and c = 7.8228 Å. These lattice parameters are lower than those calculated from the JCPDS file. This difference is believed to be due to the in-plane tensile stress applied on the film by the silicon substrate because of the thermal expansion mismatch between the film and substrate.

The electrical resistivity of SRO thin films is severely affected by their microstructure, including crystallinity, grain size, grain boundary, and density. Although similar diffraction intensities were observed for SRO films made at different crystallization temperatures, SEM revealed a marked difference in their surface microstructure, as demonstrated in Figure 5. These images indicate that the films become denser, more homogeneous, and well connected with increasing crystallization temperature. At 600 and 650 °C, the structure of the film is porous and appears to be an agglomeration of individual grains compared to the films made above 700 °C, where they appear to be denser and well connected. The aerial density, calculated from these images using ImageJ software, increased from 86.5 to 93.2% when the crystallization temperature increased from 600 to 750 °C. The average grain size was $<$100 nm and did not vary much with increasing crystallization temperature. The insignificant variation in the grain size is also implied from the fact that the FWHM calculated for the (121) peaks (in Figure 4) ranged between 0.38 and 0.39° for these films. Cross-sectional SEM revealed a thickness of ~0.3 μm for a typical five-layer SRO film on silicon.

The electrical resistivity of SRO films crystallized at different temperatures is presented in Figure 6. More than

(24) Borchardt, H. J.; Daniels, F. *J. Am. Chem. Soc.* **1957**, *79*, 41.
(25) Banerjee, A.; Prasad, R.; Venugopal, V. *J. Alloys Compd.* **2003**, *353*, 263.
(26) Jacob, K. T.; Lwin, K. T.; Waseda, Y. *Mater. Sci. Eng., B* **2003**, *103*, 152.
(27) Lide D. R. *CRC Handbook of Chemistry and Physics*, 75th ed.; CRC Press: Boca Raton, FL, 1995; pp 5-73−5-75.

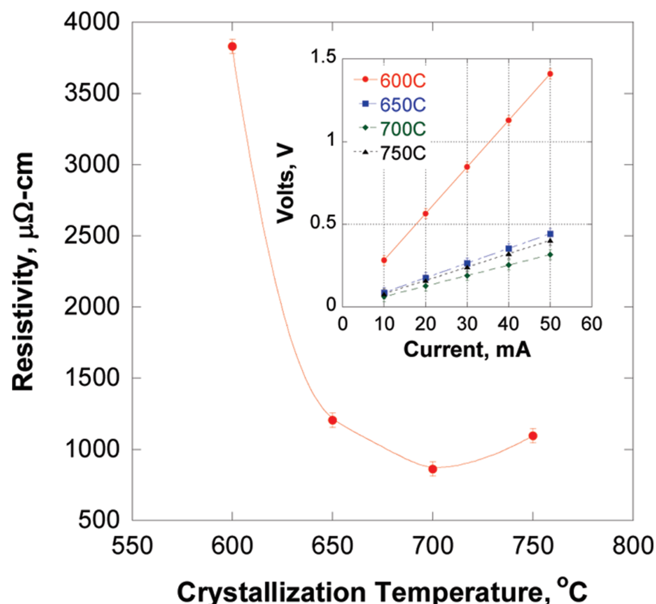

Figure 6. Calculated room temperature resistivity of SRO films crystallized at different temperatures. Inset shows the measured voltage for various currents applied using the four-point probe method for films crystallized at 600−750 °C.

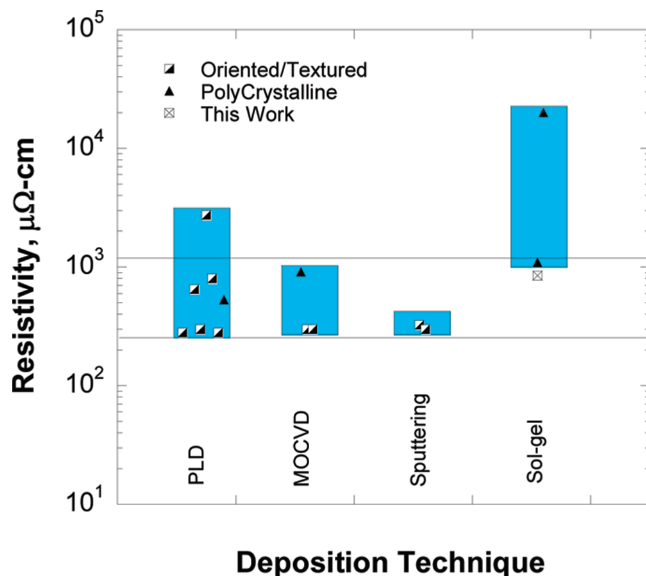

Figure 7. Resistivity of oriented/textured and polycrystalline SRO thin films fabricated by different techniques reported in the literature. Horizontal lines represent the resistivity values of 280 $\mu\Omega$ cm[30] and 1130 $\mu\Omega$ cm[28, 29] in single-crystal and polycrystalline SRO bulk ceramics.

ten measurements were performed for each temperature, and the average resistivity is plotted. The inset in Figure 6 shows the measured voltage for various currents applied by using the four-point probe method for films crystallized at 600−750 °C. The resistivity was calculated from the slope of the plots in the inset. As evident in this figure, the resistivity drops rapidly with increasing crystallization temperature, achieving a minimum value of ~850 ± 50 $\mu\Omega$ cm for films grown at 700 °C. This behavior is attributed to the improved density and connectivity in the films, which is confirmed by SEM images in Figure 5. The increase in crystalline nature of SRO film was confirmed

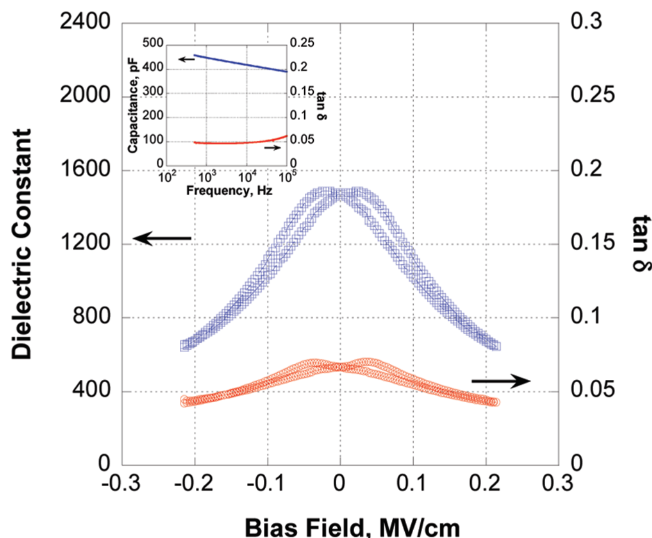

Figure 8. Room-temperature dielectric response measured at 10kHz as a function of bias voltage for a ~0.7 μm thick PLZT(8/52/48) film on ~0.3 μm thick SRO-buffered silicon substrate. Inset shows the capacitance and tan δ as a function of frequency for the PLZT/SRO/Si capacitor.

by above-mentioned XRD patterns. The minimum resistivity measured is lower than 1130 $\mu\Omega$ cm[28,29] for bulk polycrystalline SRO but higher than 280 $\mu\Omega$ cm[30] for single-crystal SRO reported in the literature. As shown in Figure 6, the resistivity for the SRO films started to increase beyond 700 °C, and this increase is speculated to be due to silicon diffusion into the film.[20] The resistivity values reported in the literature for oriented/textured and polycrystalline SRO thin films fabricated by different techniques are illustrated in Figure 7. In general, the oriented/textured films exhibit much lower resistivities than polycrystalline films. The resistivity measured in this work is the lowest value that has been reported for polycrystalline SRO films formed by sol−gel synthesis and is comparable to that of films made by PLD and MOCVD. The lowest-resistivity crystallization temperature of 700 °C for SRO films was used in further experiments and is considered to be the optimized processing condition. The observed microstructure and electrical properties were not significantly altered because of solution aging.

Although the characterization techniques mentioned above give useful information regarding the electrode material, the ultimate test of the quality of the films lies in the dielectric properties of ferroelectric thin films like PZT, BST, or PLZT deposited over the bottom oxide electrode. Such experiments would give direct evidence on the performance, compatibility, and integrity of the bottom SRO electrodes in actual devices for different applications. As a result, we deposited PLZT 8/52/48 thin films on SRO-buffered silicon substrates and characterized their dielectric properties to verify the quality of the underlying SRO bottom electrode.

(28) Chu, F.; Jia, Q. X.; Landrum, G.; Wu, X. D.; Hawley, M; Mitchell, T. E. *J. Electron. Mater.* **1996**, *25*, 1754.
(29) Nora, Y.; Miyahara, S. *J. Phys. Soc. Jpn.* **1969**, *27*, 518.
(30) Bouchard, R. J.; Gillson, J. L. *Mater. Res. Bull.* **1972**, *7*, 873.

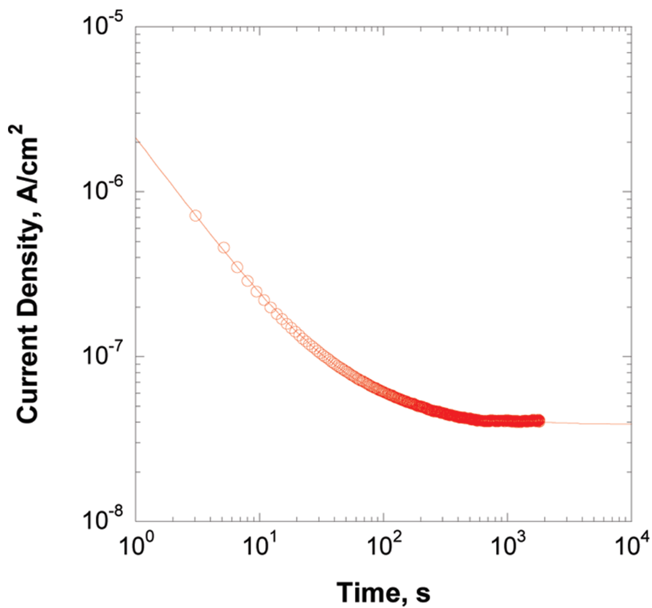

Figure 9. Leakage current density as function of time for 0.7 μm thick PLZT film on ~0.3 μm thick SRO-buffered silicon substrate for an applied field of ~90 kV/cm at room temperature.

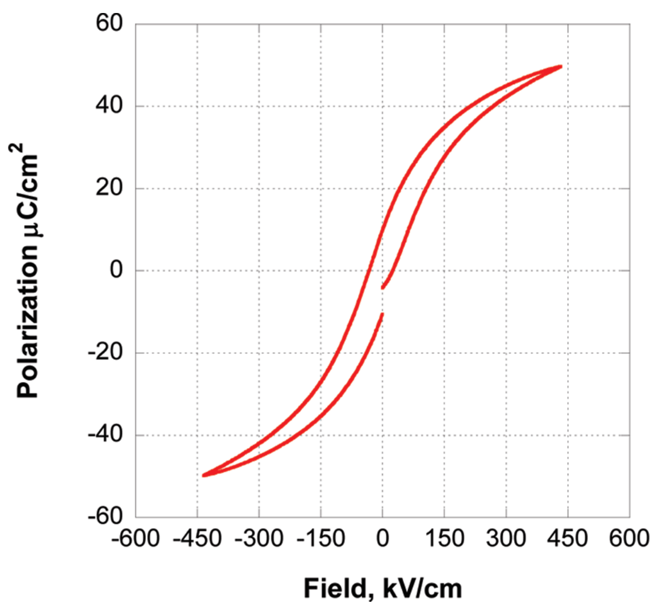

Figure 10. Polarization-field hysteresis loops of PLZT on SRO-buffered silicon samples.

The dielectric response as a function of bias voltage for PLZT films deposited on optimized SRO-buffered silicon substrates is illustrated in Figure.8. These films exhibit well-defined hysteresis, saturation at high electric field, and good dielectric tunability. A dielectric constant (k) of ~1450, dielectric loss (tan δ) of < 0.06, and dielectric tunability of ~55% were typically observed for these films on SRO-buffered silicon. The measured dielectric values are comparable to those reported for PLZT on Pt−Si ($k \approx 1450$, tan δ < 0.04)[31]and on $LaNiO_3$-buffered nickel ($k \approx 1300$, tan δ < 0.06[15,31]) substrates processed

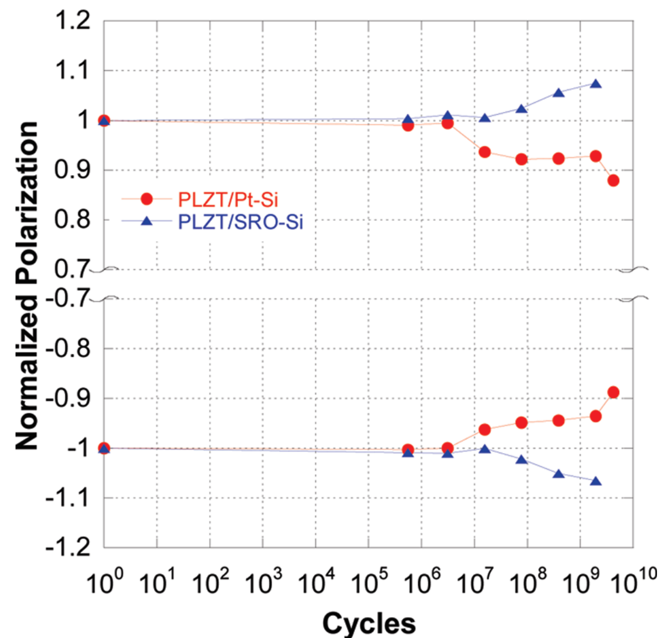

Figure 11. Polarization fatigue of PLZT 8/52/48 on platinum and SRO-buffered silicon substrate.

in air. The inset in Figure 8 shows the capacitance and dielectric loss as a function of frequency up to 100 kHz. The relatively flat response of the capacitance and loss can be readily observed in the figure, indicating the lack of electrode contribution to the dielectric loss, especially at high frequencies. These results signify the high quality of the conductive SRO bottom electrode and its structural compatibility with PLZT dielectric films.

Figure 9 shows the time relaxation for the current density measured at room temperature on PLZT/SRO-Si capacitors (~0.7 μm thick PLZT) with a constant bias field of ~90 kV/cm across the capacitor. The films exhibit strong initial time dependence, indicating depolarization. The decay in the dielectric relaxation current obeys the Curie−von Schweidler law,[10]

$$J = J_s + J_o \times t^{-n} \tag{2}$$

where J_s is the steady-state current density, J_0 is a fitting constant, t is the relaxation time in seconds, and n is the slope of the log−log plot. Fitting the data to eq 2, we found an n value of 0.99 and leakage current densities of (J_s) ~3.8 × 10^{-8} A/cm^2. This value is an order of magnitude higher than that of PLZT films made on $LaNiO_3$-buffered nickel substrates reported previously[15] and is currently under investigation.

The polarization-field ($P-E$) loop measured on a PLZT/SRO/Si sample at 1 kHz with a maximum applied field of 450 kV/cm is shown in Figure.10. It can be noticed that the dielectric film exhibits a well-defined hysteresis loop with coercive field, saturation polarization, and remnant polarization values of 44.6 kV/cm, 49.7 μC/cm^2, and 10.2 μC/cm^2, respectively. Figure 11 illustrates the fatigue characteristics of a typical Pt/PLZT/SRO/Si capacitor, in comparison with a Pt/PLZT/Pt/Si capacitor fabricated under the same conditions. The Pt/PLZT/Pt/Si exhibits

(31) Ma, B.; Kwon, D. K.; Narayanan, M.; Balachandran, U. *Mater. Lett.* **2008**, *62*, 3573.

the normal polarization behavior expected of platinum-based electrodes, i.e., a decrease in the polarization response beyond 1×10^6 to 1×10^7 cycles. However, the capacitor based on the SRO oxide electrode does not exhibit this fatigue. This indicates that the SRO thin films can be used as electrodes to improve fatigue resistance in memory applications. Various reports suggest a reduction in the concentration of oxygen vacancies near the oxide electrodes as the possible reason for the improved fatigue resistance.[32−34] The apparent increase in polarization with number of cycles in Pt/PLZT/SRO/Si has been commonly observed with other oxide electrodes, in particular, where leakage current increases during the fatigue process.[35−37] The polarization decreased by 12% for Pt/PLZT/Pt/Si, whereas it increased by 7% for Pt/PLZT/SRO/Si after 1×10^9 cycles. The fatigue rate for Pt/PLZT/Pt/Si in Figure 11 is lower than that reported in the literature, but the fatigue rate is highly dependent on the test conditions (frequency and field) and composition and doping elements of the PZT. The results from the dielectric characterization shown in Figure 8 through Figure 11 signify the superior quality of the underlying SRO electrode and its suitability for various applications.

Although certain applications may require oriented SRO thin films for epitaxial growth of thin-film perovskite ferroelectrics, preparing such films by sol−gel synthesis depends on various factors like solution chemistry, choice of single-crystal substrate, pyrolysis/crystallization conditions (temperature and time), and rate of heating. A detailed study on achieving oriented SRO films using the solution chemistry presented here by varying the process parameters is beyond the scope of this paper and is a topic for future study. The solution chemistry presented in this paper shows promise for such a study because of its robust crystallization behavior to form SRO without the tendency to form other secondary phases like RuO_2. This behavior gives more flexibility to alter the processing parameters to achieve oriented or textured thin films.

4. Conclusions

In summary, we have developed a new sol−gel solution chemistry for fabricating high-quality polycrystalline SRO thin films on silicon substrates by proper choice of precursor and solvents. Differential thermal analyses of the precursor and stock solutions suggested that the transformation pathway to form SRO does not favor RuO_2 phase formation due to the molecular modification of the precursors in solution during synthesis to form a homogeneous gel-network containing both the metallic species. Kinetic and thermodynamic analysis of the DTA data under nonisothermal conditions was carried out to determine the activation energy involved in the formation of the oxides. The activation energies to form RuO_2 and SRO were calculated to be 156 ± 17 and 96 ± 10 kJ/mol, respectively, suggesting that it is easier to form SRO than RuO_2. This characteristic of the solution chemistry allows the use of a higher pyrolysis temperature ($\leq$450 °C) than that historically reported to remove organics moieties in SRO films without the formation of RuO_2 and improve film density (reduce porosity). Thus, the process and crystallization conditions developed are robust for the formation of phase pure SRO. The room-temperature resistivity of SRO films fabricated on Si(100) substrates is around $\sim 850 \pm 50$ $\mu\Omega$ cm. This value is least reported value in the literature using sol−gel synthesis and comparable to that of polycrystalline films made using PLD and MOCVD. The enhanced conductivity of the films is attributed to the improved microstructure of the films.

This work also investigated the dielectric properties of sol−gel-derived PLZT thin film capacitors with polycrystalline SRO electrodes. These properties were found to be comparable with those of PLZT films on platinized silicon substrates. The PLZT (8/52/48) films formed on SRO-buffered silicon substrates exhibited well-defined hysteresis loops with remanent polarization of $\sim$10.5 $\mu C/cm^2$, dielectric constant of >1450, dielectric loss of <0.06, and leakage current density of $\sim 3.8 \times 10^{-8}$ A/cm^2. These dielectric properties are similar to those for PLZT on platinized silicon, indicating the high quality of the bottom conductive oxide layer. The PLZT capacitors deposited over the SRO electrode were essentially fatigue free for $> 1 \times 10^9$ cycles, proving that these electrodes can be used in ferroelectric RAM memory. These results also have broad implications for the expanded use of these conductive oxide electrodes in many other applications that require low thermal budgets.

Acknowledgment. Work funded by the U.S. Department of Energy, Office of Vehicle Technologies Program, under Contract DEAC02-06CH11357. The electron microscopy was accomplished at the Electron Microscopy Center for Materials Research at Argonne National Laboratory, a U.S. Department of Energy Office of Science Laboratory operated under Contract DE-AC02-06CH11357 by UChicago Argonne, LLC. Special thanks to Dr. Robert W. Schwartz at Missouri University of Science and Technology, Rolla, MO, and Dr. Wei Li (MSD) at Argonne National Laboratory for their valuable comments on the manuscript.

(32) Damjanovic, D. *Rep. Prog. Phys.* **1998**, *61*, 1267.
(33) Paz de Araujo, C. A.; Cuchiaro, J. D.; McMillan, L. D.; Scott, M. C.; Scott, J. F. *Nature* **1995**, *374*, 627.
(34) Dawber, M.; Rabe, K. M.; Scott, J. F. *Rev. Mod. Phys.* **2005**, *77*, 1083.
(35) Bernstein, S. D.; Wong, T. Y.; Kisler, Y.; Tustison, R. W. *J. Mater. Res.* **1993**, *8*, 12–13.
(36) Al-Shareef, H. N.; Kingon, A. I.; Chen, X.; Bellur, K. R.; Auciello, O. *J. Mater. Res.* **1994**, *9*, 2968.
(37) Al-Shareef, H. N.; Auciello, O.; Kingon, A. I. *J. Appl. Phys.* **1995**, *77*, 2146.